Geochronology, 1, 69–84, 2019
https://doi.org/10.5194/gchron-1-69-2019

Exploring the advantages and limitations of in situ U–Pb carbonate geochronology using speleothems

Jon Woodhead[1] **and Joseph Petrus**[2]

[1]School of Earth Sciences, University of Melbourne, Melbourne, VIC 3010, Australia
[2]Harquail School of Earth Sciences, Laurentian University, Sudbury, Canada

Correspondence: Jon Woodhead (jdwood@unimelb.edu.au)

Received: 8 July 2019 – Discussion started: 16 July 2019
Revised: 5 November 2019 – Accepted: 11 November 2019 – Published: 5 December 2019

Abstract. The recent development of methods for in situ U–Pb age determination in carbonates has found widespread application, but the benefits and limitations of the method over bulk analysis (isotope dilution – ID) approaches have yet to be fully explored. Here we use speleothems – cave carbonates such as stalagmites and flowstones – to investigate the utility of in situ dating methodologies for "challenging" matrices with typically low U and Pb contents and predominantly late Cenozoic ages. Using samples for which ID data have already been published, we show that accurate ages can be obtained for many speleothem types by laser ablation inductively coupled plasma mass spectrometry (LA-ICPMS). Consideration of our own and literature data suggest that most carbonates with > 1 ppm uranium and a few hundred parts per billion of Pb should be good targets for in situ methodologies, regardless of age. In situ analysis often provides a larger spread in U/Pb ratios, which can be advantageous for isochron construction, but isochron ages rarely achieve the ultimate precision of ID analyses conducted on the same samples simply because signal sizes are dramatically reduced. LA analysis is faster than ID and thus will play a significant role in reconnaissance studies. The major advantage of the in situ methodology appears to be the potential for successful dating outcomes in sample types requiring high spatial-resolution analysis or those with a high common-Pb component where LA approaches may facilitate identification of the most radiogenic regions for analysis.

1 Introduction

The U–Pb decay scheme has played a key role in the chronology of carbonate rocks for more than 3 decades (e.g. Moorbath et al., 1987; Jahn and Cuvellier, 1994; Rasbury and Cole, 2009) utilizing predominantly isotope dilution (ID; i.e. bulk sample) methods. Recent years, however, have seen a revolution in the field with the emergence of in situ analysis techniques employing laser ablation inductively coupled plasma mass spectrometry (LA-ICPMS) and offering the prospect of direct determination of U–Pb ages on the scale of a few hundred microns. Although still in its infancy, this method has already been applied to the chronology of marine cements (Li et al., 2014), vein calcites associated with faulting (Roberts and Walker, 2016; Hansman et al., 2018; Parrish et al., 2018), and the alteration of oceanic crust (Coogan et al., 2016).

To date, a thorough exploration of the utility of in situ techniques to speleothem (secondary cave calcite such as stalagmites and flowstones) research has not been conducted, although U–Pb dating of speleothems is widely used in studies of climate change (e.g. Vaks et al., 2013; Sniderman et al., 2016), human evolution and migration (e.g. Walker et al., 2006; Pickering et al. 2011, 2019), bio-diversity and ecosystem change (e.g. Woodhead et al., 2016), and tectonics and landscape evolution (e.g. Lundberg, 2000; Polyak et al., 2008; Meyer et al., 2011; Woodhead et al., 2019). Speleothems offer a variety of unique analytical challenges for in situ analysis – not least because of their highly variable and often very low levels of radiogenic Pb, but also because of the fact that most samples of interest are also relatively young – predominantly Neogene or early Quaternary.

As such they actually form a useful test of the limitations of the in situ carbonate dating methodology more generally. Here we explore the utility of LA-ICPMS techniques as applied to speleothems not only to highlight important new research avenues but also to explore both the benefits and limitations of the method.

We first compare LA-ICPMS (henceforth "LA") ages for a variety of speleothem samples for which bulk, solution multi-collector ICPMS, ID U–Pb age data have already been published as a benchmark against which to judge the reliability of our in situ analyses. We then explore the advantages and limitations of LA methodologies in this context and make recommendations for the optimal use of both technologies.

2 Materials and methods

2.1 Overview

Samples for analysis were prepared either as polished slabs or Epofix™ resin mounts. While a polished surface is not an essential prerequisite for LA studies, it significantly enhances the ability to view the sample clearly with the reflected light microscopes widely employed in LA systems. Mounts were cleaned in ultra-pure water in an ultrasonic bath and dried under nitrogen prior to loading into the sample cell.

We used the "freeform" sample holder available in the S155 large-format ablation cell of an Australian Scientific Instruments (now Applied Spectra) RESOlution-LR ablation system, based around a Lambda Physik Compex 110 excimer laser, operating at 193 nm wavelength, and coupled to a Nu Instruments Attom-ES high-resolution magnetic sector ICPMS operating in deflector jump mode.

Laser fluence was typically adjusted to $\sim$ 2–3 J cm^{-2}, and we used a laser repetition rate of 5 Hz, allowing the potential for depth resolution if required (see below). Analyses were conducted with either a 154 µm or 228 µm spot; we aimed to achieve maximum ^{207}Pb counts, without taking ^{238}U into attenuated mode (the first attenuation mode trip on our instrument was set to 3 million cps (counts per second) for this study). A brief pre-ablation using a larger spot size was conducted prior to every analysis. Baseline measurement for 30 s was followed by 40 s acquisition during each spot ablation. The masses measured and dwell times used are documented in Table 1, together with other instrumental parameters. Laser gas flows and instrument settings were optimized primarily for highest sensitivity: for a 40 µm spot under these conditions on a NIST glass, we see around 25–35 000 cps ppm^{-1}. Although oxide levels are generally low (^{248}ThO/^{232}Th < 0.3 %), and Th/U ratios close to unity, we have observed no relationship between variation in these parameters and data quality, and do not tune to optimize these values (as is commonplace, for example, in trace element determination). Table 2 lists the samples used in these experiments and the publications in which original ID data for these materials (reproduced in Table 3) can be found.

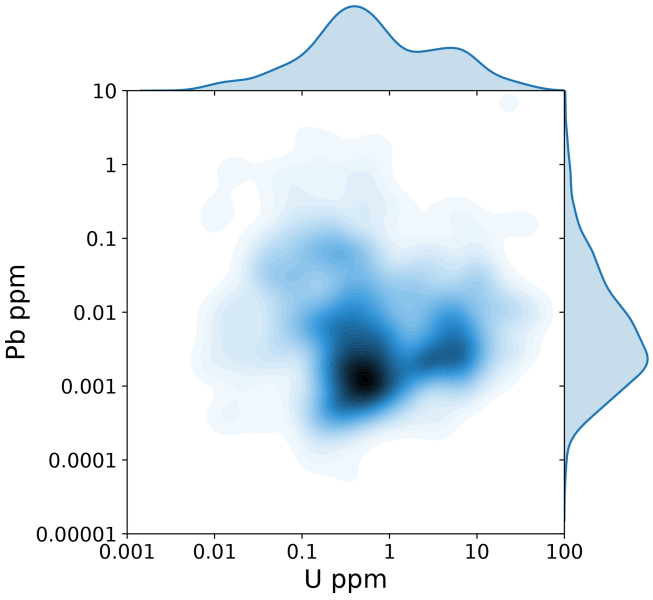

Figure 1. Speleothem U and Pb concentrations. Two-dimensional Kernel density plot of U and Pb concentration data obtained by ID methods in our laboratory over the past decade, representing over 2000 sample aliquots. All samples were leached briefly in dilute HCl prior to dissolution to remove any blank Pb that may have been introduced during sample handling (e.g. Woodhead et al., 2012). The small hotspot to the right of the main array is dominated by the Corchia site in Italy, from which we have analysed many samples. The vast majority of other speleothems, however, have 0.1–1 ppm U and $\sim$ 0.001 ppm Pb.

2.2 Analytical strategies

Natural speleothems display a remarkably wide range of U and Pb concentrations – Fig. 1 shows data generated for over 2000 speleothem calcite aliquots analysed at the University of Melbourne by ID methods over a 10-year period following rigorous sample cleaning protocols to remove Pb contaminants derived from initial processing (e.g. Woodhead et al., 2012). The majority of samples contain $\sim$ 0.1–10 ppm U and generally very low Pb concentrations, typically $\sim$ 1–100 ppb. These traits provide very challenging conditions for LA analysis.

The primary concern for any samples of this type, and particularly when measuring by LA, is the obvious potential for contamination with environmental ("blank") Pb during analysis. Although LA rastering and extraction of age information from the resulting isotopic images have shown great promise for dating limestones with relatively high Pb abundances (Drost et al., 2018), the same approach cannot be easily implemented in speleothems where Pb contents are often in the low parts per billion range and thus where each spot analysis may be measuring total Pb amounts in the low femtogram range. For this reason, in this study, we have used spot analyses and perform a clean pre-ablation with a larger

Table 1. Instrumental parameters.

Laser ablation system	
Manufacturer and model	Australian Scientific Instruments (now Applied Spectra) RESOlution-LR
Ablation cell	S155 large format cell
Laser wavelength (nm)	193 nm
Pulse width (ns)	20 ns
Fluence	$\sim$ 2–3 J cm^{-2}
Repetition rate (Hz)	5 Hz
Spot size (µm)	154 or 228 µm
Sampling mode or pattern	Static spot
Cell gases	Sample ablated into pure helium but then rapidly (within 1 cm) entrained into argon flow within the ablation volume
Ablation conditions	30 s baseline measurement followed by 40 s ablation
Cell gas flows (L min^{-1})	0.25 helium, 0.8–0.9 Ar (tuned for maximum sensitivity, not low oxides)
ICPMS instrument	
Make, model, and type	Nu Instruments, Attom-ES high-resolution ICPMS used in deflector jump mode
RF (radio frequency) power (W)	1300 W
Make-up gas flow	0.7 L min^{-1} Ar
Detection system	Single Mascom SEM (secondary electron multiplier)
Masses measured	206, 207, 208, 232, 235, 238
Integration time on peak	206 (2 ms), 207 (2 ms), 208 (200 µs), 232 (200 µs), 235 (200 µs), 238 (1 ms)
Time per cycle (s)	0.125 s
IC (ion counter) dead time (ns)	17 ns
Data processing	
Gas blank	30 s on-peak zero subtracted using Iolite smoothing spline
Calibration strategy	WC-1 carbonate
Data processing package used or correction for LIEF	UcomPbine DRS vs. 2015.06 running in Iolite vs. 3.71 providing baseline subtraction, downhole correction and calibration against the reference material; the ^{207}Pb-based common-Pb method was employed.
Uncertainty level and propagation	Ages are quoted at 2σ absolute; data are presented with measurement precision only.

Table 2. Samples utilized in this study. Mean U and Pb contents are the averages of the isotope dilution data reported in the appropriate publications. In order to allow direct comparison with the LA data none of the ID ages quoted below include a correction for initial disequilibrium in the U–Pb decay chain: as such the ages shown for the two youngest samples differ slightly to those reported in the publications.

Sample ID	Location	Mean U parts per million	Mean Pb parts per million	ID age (Ma)	Reference
P-1	Richard's Spur, Oklahoma, USA	0.206	0.016	289 ± 1	Woodhead et al. (2010)
RSO	Riversleigh World Heritage fossil site, Queensland, Australia			16.55 ± 0.31	Woodhead et al. (2016)
0708	Riversleigh World Heritage fossil site, Queensland, Australia	1.43	0.006	13.72 ± 0.12	Woodhead et al. (2016)
0708g	Riversleigh World Heritage fossil site, Queensland, Australia	1.39	0.006	13.48 ± 0.45	Woodhead et al. (2016)
LBCT-01	Nullarbor Plain, SW Australia	2.69	0.004	3.246 ± 0.002	Woodhead et al. (2019)
M-01	Nullarbor Plain, SW Australia	1.04	0.002	3.699 ± 0.001	Woodhead et al. (2006)

Table 3. Isotope data used in the construction of Fig. 3. To provide consistency with the LA data, the ID uncertainties have been converted to "absolute" from the "%" values quoted in the original publications.

LA data					ID data				
$^{238}U/^{206}Pb$	2σ abs.	$^{207}Pb/^{206}Pb$	2σ abs.	error corr.	$^{238}U/^{206}Pb$	2σ abs.	$^{207}Pb/^{206}Pb$	2σ abs.	error corr.
Sample P-1									
16.21	0.68	0.258	0.024	0.108	19.31	0.13	0.139	0.005	−0.998
19.86	0.39	0.135	0.016	−0.031	19.60	0.27	0.128	0.011	−0.998
18.21	0.70	0.162	0.014	−0.006	19.15	0.09	0.148	0.004	−0.997
17.73	0.57	0.195	0.021	0.141	13.80	0.05	0.338	0.002	−0.995
18.66	0.56	0.163	0.014	0.225	16.81	0.07	0.230	0.003	−0.997
19.34	0.56	0.145	0.020	0.041	13.97	0.10	0.329	0.004	−0.996
20.55	0.38	0.106	0.011	0.108	16.44	0.13	0.242	0.005	−0.997
19.21	0.33	0.168	0.010	0.073	20.03	0.10	0.115	0.004	−0.994
19.16	0.37	0.167	0.011	0.113	20.12	0.07	0.112	0.003	−0.995
19.76	0.39	0.125	0.007	0.217	20.26	0.05	0.108	0.002	−0.967
20.06	0.36	0.113	0.010	−0.005	17.24	0.04	0.216	0.002	−0.982
17.30	0.60	0.199	0.016	0.225					
19.57	0.46	0.144	0.010	0.091					
18.05	0.49	0.198	0.018	0.091					
17.79	0.44	0.174	0.012	0.117					
16.47	0.46	0.229	0.018	−0.201					
18.83	0.46	0.149	0.011	0.155					
20.04	0.44	0.139	0.021	0.153					
19.27	0.63	0.150	0.019	0.001					
18.12	0.72	0.208	0.046	0.128					
17.76	0.47	0.227	0.015	0.223					
19.31	0.37	0.175	0.014	0.171					
20.45	0.46	0.135	0.014	−0.036					
16.56	0.44	0.205	0.011	0.323					
14.92	0.20	0.325	0.010	0.276					
19.80	0.63	0.148	0.016	0.062					
19.05	0.47	0.170	0.019	0.242					
15.20	0.55	0.308	0.020	−0.128					
17.99	0.68	0.271	0.041	0.056					
19.23	0.52	0.148	0.018	−0.115					
20.38	0.37	0.106	0.007	0.199					
19.42	0.60	0.148	0.017	0.075					
20.28	0.58	0.090	0.014	0.102					
19.34	0.41	0.140	0.009	0.123					
20.28	0.45	0.106	0.012	0.048					
19.27	0.37	0.147	0.009	0.152					
19.72	0.43	0.182	0.018	0.041					
17.54	0.46	0.170	0.014	0.140					
18.76	0.53	0.173	0.018	0.086					
16.56	0.79	0.268	0.041	0.026					
19.19	0.44	0.163	0.020	0.040					
19.16	0.36	0.155	0.018	0.099					
18.62	0.45	0.177	0.022	0.048					
17.04	0.49	0.213	0.028	0.131					
18.90	0.43	0.191	0.017	0.054					
20.00	0.56	0.136	0.018	0.071					
17.15	0.32	0.225	0.010	0.249					
17.06	0.44	0.245	0.024	0.041					
18.69	0.45	0.160	0.021	0.056					
19.12	0.44	0.155	0.017	0.107					
19.57	0.54	0.142	0.015	0.190					
19.27	0.41	0.172	0.017	0.110					
19.61	0.42	0.134	0.010	0.114					

Table 3. Continued.

LA data					ID data				
$^{238}U/^{206}Pb$	2σ abs.	$^{207}Pb/^{206}Pb$	2σ abs.	error corr.	$^{238}U/^{206}Pb$	2σ abs.	$^{207}Pb/^{206}Pb$	2σ abs.	error corr.
13.04	0.42	0.375	0.024	0.091					
19.76	0.59	0.154	0.024	−0.150					
14.99	0.52	0.362	0.035	−0.049					
17.27	0.39	0.245	0.014	0.121					
17.24	0.62	0.203	0.016	0.288					
18.62	0.52	0.170	0.011	0.290					
17.57	0.65	0.223	0.024	0.174					
19.50	0.34	0.162	0.010	−0.021					
16.67	0.47	0.256	0.018	0.145					
18.69	0.45	0.173	0.018	0.026					
17.92	0.55	0.227	0.019	0.038					
19.57	0.46	0.127	0.010	−0.013					
18.59	0.41	0.201	0.016	0.055					
19.34	0.37	0.182	0.019	−0.003					
16.47	0.54	0.217	0.017	−0.020					
17.39	0.57	0.220	0.025	0.233					
Sample RSO									
7.03	0.05	0.771	0.008	0.372	30.70	0.06	0.718	0.000	−0.972
13.32	0.25	0.755	0.010	0.391	26.82	0.07	0.725	0.000	−0.846
69.35	1.64	0.683	0.028	0.261	29.74	0.06	0.719	0.000	−0.966
188.68	4.27	0.415	0.017	0.377	25.28	0.07	0.728	0.000	−0.962
85.32	1.38	0.648	0.019	0.002	32.75	0.04	0.714	0.001	−0.847
1.12	0.01	0.782	0.003	0.260	34.73	0.05	0.710	0.001	−0.828
139.47	2.92	0.504	0.016	0.496	42.31	0.05	0.696	0.001	−0.887
81.57	1.13	0.631	0.015	0.575					
12.74	0.10	0.761	0.008	0.529					
116.41	5.42	0.549	0.019	−0.077					
1.85	0.01	0.785	0.003	0.206					
166.11	3.31	0.475	0.018	−0.003					
201.61	5.28	0.406	0.019	0.226					
100.70	1.72	0.606	0.016	0.539					
2.33	0.02	0.778	0.004	0.119					
112.61	2.66	0.574	0.016	0.304					
9.48	0.08	0.767	0.008	0.354					
4.67	0.04	0.774	0.006	0.688					
230.95	6.93	0.372	0.021	0.360					
111.98	5.39	0.531	0.020	−0.360					
36.06	0.47	0.711	0.012	0.162					
10.65	0.12	0.771	0.010	0.649					
105.60	1.78	0.571	0.015	0.481					
20.85	0.22	0.745	0.011	0.480					
163.93	5.37	0.450	0.023	0.161					
41.12	0.46	0.717	0.010	0.493					
101.73	1.66	0.594	0.016	0.489					
6.98	0.07	0.775	0.007	0.397					
65.45	0.77	0.669	0.013	0.305					
14.06	0.18	0.764	0.008	0.258					
7.77	0.06	0.772	0.005	0.308					
23.09	0.59	0.737	0.010	0.060					
7.90	0.06	0.775	0.006	0.391					
114.16	2.74	0.589	0.020	0.263					
78.74	1.43	0.636	0.014	0.378					
143.06	2.66	0.531	0.018	0.526					
169.78	3.75	0.455	0.020	0.520					
167.50	3.93	0.494	0.019	0.274					

Table 3. Continued.

LA data					ID data				
$^{238}U/^{206}Pb$	2σ abs.	$^{207}Pb/^{206}Pb$	2σ abs.	error corr.	$^{238}U/^{206}Pb$	2σ abs.	$^{207}Pb/^{206}Pb$	2σ abs.	error corr.
43.23	0.77	0.702	0.012	0.611					
34.20	0.58	0.722	0.013	0.396					
138.89	2.70	0.514	0.015	0.608					
10.52	0.17	0.771	0.008	0.183					
28.11	0.41	0.742	0.010	0.110					
125.94	2.22	0.549	0.016	0.475					
5.78	0.05	0.775	0.007	0.395					
12.22	0.15	0.762	0.008	0.260					
98.72	1.75	0.601	0.015	0.419					
70.03	2.55	0.633	0.015	0.118					
41.27	0.46	0.717	0.012	0.681					
Sample 0708									
73.21	2.25	0.753	0.015	−0.068	368.42	4.17	0.221	0.008	−0.995
260.42	8.14	0.435	0.020	0.189	360.84	2.62	0.234	0.005	−0.996
169.20	4.87	0.577	0.020	0.456	349.58	3.93	0.251	0.007	−0.997
79.18	1.82	0.751	0.020	0.196	413.09	13.63	0.145	0.025	−0.999
212.77	5.89	0.473	0.017	0.375	339.01	4.27	0.266	0.008	−0.996
154.56	3.58	0.615	0.021	0.226	320.57	3.90	0.298	0.007	−0.881
217.39	5.67	0.474	0.019	0.279					
209.64	9.67	0.484	0.022	0.110					
144.09	4.98	0.647	0.021	0.102					
174.22	3.95	0.584	0.018	0.214					
224.22	6.54	0.477	0.024	0.265					
236.41	6.71	0.461	0.023	0.147					
161.55	5.74	0.628	0.022	−0.041					
265.25	11.26	0.385	0.023	−0.043					
152.44	4.65	0.608	0.019	0.020					
151.75	4.61	0.626	0.021	0.003					
101.11	2.35	0.727	0.017	0.038					
265.18	6.82	0.427	0.019	0.070					
286.78	6.33	0.391	0.017	0.241					
287.60	7.11	0.365	0.016	−0.041					
264.69	5.67	0.419	0.016	0.159					
274.57	5.35	0.378	0.016	0.177					
212.31	8.56	0.501	0.026	0.341					
161.29	3.38	0.591	0.018	0.144					
140.65	3.17	0.633	0.021	0.188					
183.15	4.36	0.557	0.021	0.494					
218.82	4.79	0.530	0.024	0.217					
312.50	10.74	0.334	0.020	−0.081					
227.79	4.41	0.490	0.021	0.073					
212.77	5.43	0.507	0.022	0.255					
139.28	4.07	0.652	0.020	0.449					
179.53	4.51	0.556	0.021	0.243					
224.22	5.03	0.480	0.017	0.112					
219.78	7.25	0.519	0.023	0.313					
165.02	5.72	0.590	0.023	0.036					
145.77	4.67	0.610	0.021	0.099					
239.81	8.05	0.442	0.019	−0.105					
187.27	5.61	0.538	0.025	0.119					
255.23	5.28	0.443	0.017	0.026					
141.44	8.20	0.616	0.022	−0.155					
115.34	2.00	0.707	0.020	0.151					

Table 3. Continued.

LA data					ID data				
$^{238}U/^{206}Pb$	2σ abs.	$^{207}Pb/^{206}Pb$	2σ abs.	error corr.	$^{238}U/^{206}Pb$	2σ abs.	$^{207}Pb/^{206}Pb$	2σ abs.	error corr.
117.51	2.35	0.680	0.016	0.339					
73.64	1.25	0.757	0.013	0.579					
160.26	4.62	0.605	0.024	0.164					
149.70	3.14	0.619	0.018	0.246					
245.28	5.17	0.452	0.016	0.337					
251.26	8.21	0.435	0.028	0.359					
130.21	4.24	0.666	0.022	0.184					
276.24	8.39	0.419	0.020	0.167					
298.51	9.80	0.359	0.021	−0.091					
381.68	12.82	0.241	0.026	0.007					
Sample 0708g									
77.10	1.13	0.738	0.014	0.550	372.78	3.95	0.214	0.007	−0.995
171.23	7.62	0.560	0.025	0.330	369.19	4.37	0.219	0.008	−0.997
142.25	3.64	0.591	0.019	0.343	360.24	6.12	0.240	0.011	−0.983
146.41	5.79	0.636	0.029	0.484	369.71	6.91	0.221	0.013	−0.995
167.22	3.64	0.539	0.020	0.430	349.12	10.00	0.255	0.019	−0.999
77.70	2.66	0.729	0.033	0.262	346.40	3.31	0.255	0.006	−0.998
139.47	2.92	0.636	0.022	0.341	396.79	6.13	0.182	0.011	−0.945
214.13	6.88	0.468	0.025	0.488					
129.53	3.69	0.672	0.029	0.675					
139.66	3.32	0.658	0.023	0.368					
183.49	10.44	0.550	0.030	0.534					
297.27	8.31	0.349	0.022	0.318					
172.41	3.27	0.539	0.017	0.545					
172.41	5.05	0.549	0.021	0.308					
96.90	1.50	0.693	0.020	0.218					
253.81	12.88	0.446	0.069	0.049					
59.52	1.56	0.735	0.014	0.053					
176.06	4.65	0.596	0.022	0.179					
128.87	2.66	0.663	0.018	0.259					
78.55	3.09	0.728	0.025	0.488					
190.11	7.23	0.543	0.027	0.193					
108.81	2.49	0.687	0.016	0.348					
234.74	6.61	0.489	0.023	0.344					
137.55	6.81	0.623	0.024	−0.152					
375.94	14.13	0.220	0.030	0.073					
129.37	3.68	0.685	0.029	0.360					
39.12	0.98	0.820	0.013	0.191					
235.85	10.57	0.498	0.036	0.148					
126.90	4.67	0.675	0.035	0.399					
90.66	1.64	0.730	0.017	0.189					
258.40	10.68	0.465	0.038	0.026					
198.41	9.05	0.554	0.025	−0.217					
265.96	8.49	0.416	0.023	0.356					
195.31	9.16	0.591	0.029	0.022					
151.29	3.66	0.640	0.020	0.284					
331.13	12.06	0.323	0.026	0.016					
Sample LBCT-01									
1851.85	51.44	0.124	0.016	−0.030	1906.99	34.19	0.078	0.015	−0.999
1834.86	50.50	0.135	0.018	0.218	1892.32	26.12	0.084	0.011	−0.998
1821.49	53.09	0.149	0.015	0.239	1043.17	5.09	0.431	0.002	−0.996
1324.50	40.35	0.359	0.024	0.175	1701.49	12.01	0.162	0.005	−0.992
1538.46	71.01	0.259	0.030	−0.005	1538.93	10.63	0.228	0.005	−0.992
1317.52	48.60	0.326	0.030	0.227	809.87	13.70	0.529	0.011	−0.990

Table 3. Continued.

LA data					ID data				
$^{238}U/^{206}Pb$	2σ abs.	$^{207}Pb/^{206}Pb$	2σ abs.	error corr.	$^{238}U/^{206}Pb$	2σ abs.	$^{207}Pb/^{206}Pb$	2σ abs.	error corr.
1597.44	53.59	0.250	0.023	0.192					
836.12	23.77	0.587	0.026	0.282					
1631.32	53.22	0.204	0.023	0.234					
1168.22	42.31	0.452	0.030	0.348					
1400.56	47.08	0.324	0.024	0.232					
1322.75	33.24	0.325	0.021	0.086					
1090.51	42.81	0.388	0.027	0.237					
1207.73	40.84	0.387	0.033	0.090					
1459.85	44.75	0.314	0.027	0.159					
1550.39	50.48	0.234	0.021	0.073					
983.28	29.97	0.483	0.024	0.415					
1264.22	36.76	0.333	0.023	0.227					
1291.99	48.41	0.329	0.030	0.231					
1288.66	39.86	0.364	0.023	0.056					
1329.79	37.14	0.330	0.020	0.173					
1329.79	42.44	0.312	0.026	0.265					
1390.82	38.69	0.291	0.019	0.103					
1577.29	44.78	0.227	0.019	0.216					
1492.54	40.10	0.275	0.019	0.213					
1392.76	42.68	0.309	0.024	0.208					
1007.05	24.34	0.465	0.023	0.337					
1228.50	39.24	0.353	0.021	0.176					
1222.49	32.88	0.377	0.020	0.264					
969.93	26.34	0.466	0.025	0.195					
1206.27	33.47	0.344	0.021	0.409					
858.37	19.89	0.521	0.022	0.093					
1158.75	30.88	0.400	0.022	0.354					
1015.23	39.17	0.464	0.030	0.158					
1436.78	45.42	0.291	0.022	0.191					
1658.38	55.00	0.212	0.037	0.051					
1135.07	39.94	0.480	0.037	0.333					
1631.32	50.56	0.236	0.025	0.187					
1199.04	28.75	0.364	0.020	0.249					
1340.48	34.14	0.347	0.020	0.307					
1398.60	41.08	0.277	0.019	0.261					
1377.41	36.05	0.300	0.018	0.318					
1623.38	50.07	0.223	0.019	0.070					
1524.39	55.77	0.262	0.027	0.159					
1228.50	36.22	0.417	0.027	0.279					
1703.58	60.95	0.203	0.022	0.109					
1474.93	52.21	0.246	0.019	0.201					
1492.54	42.33	0.277	0.022	0.033					
1287.00	54.66	0.353	0.030	0.475					
1319.26	34.81	0.346	0.022	0.305					
Sample M-01									
1404.49	94.69	0.117	0.065	0.506	1622.42	16.47	0.103	0.008	−1.000
1158.75	116.81	0.290	0.170	0.171	1553.76	21.66	0.136	0.011	−1.000
1366.12	74.65	0.205	0.061	0.032	337.49	1.06	0.714	0.001	−0.999
1494.77	78.20	0.174	0.045	0.051	1519.08	13.12	0.152	0.007	−0.999
1396.65	148.25	0.200	0.160	0.250	1668.61	30.95	0.081	0.015	−1.000
1666.67	102.78	0.073	0.047	0.768					
1533.74	110.56	0.197	0.097	0.267					
1584.79	130.60	0.280	0.120	0.218					
1733.10	147.18	0.180	0.110	−0.005					
1666.67	83.33	0.126	0.039	−0.056					

Table 3. Continued.

LA data					ID data				
$^{238}U/^{206}Pb$	2σ abs.	$^{207}Pb/^{206}Pb$	2σ abs.	error corr.	$^{238}U/^{206}Pb$	2σ abs.	$^{207}Pb/^{206}Pb$	2σ abs.	error corr.
1426.53	122.10	0.272	0.099	0.201					
1321.00	75.04	0.338	0.072	0.213					
1506.02	79.38	0.166	0.051	0.139					
1383.13	78.43	0.205	0.054	0.064					
1763.67	111.98	0.178	0.091	0.133					
1703.58	116.09	0.238	0.072	0.215					
1776.20	123.04	0.192	0.053	0.327					
1733.10	135.16	0.094	0.088	0.302					
1438.85	151.13	0.230	0.200	0.183					
1324.50	103.50	0.281	0.061	0.610					
1557.63	94.62	0.089	0.049	0.156					
1636.66	117.86	0.090	0.093	0.361					
1650.17	78.97	0.131	0.045	0.167					
1626.02	89.89	0.081	0.035	0.588					
1443.00	124.94	0.131	0.054	−0.057					
1552.80	106.09	0.175	0.077	0.673					
1694.92	100.55	0.064	0.058	0.766					
1490.31	133.26	0.170	0.100	0.293					
1453.49	181.69	0.064	0.082	0.465					
1610.31	101.13	0.290	0.110	0.038					
1631.32	119.75	0.209	0.088	0.684					
1686.34	105.22	0.200	0.110	−0.047					
1675.04	86.98	0.116	0.049	−0.050					
1647.45	132.99	0.148	0.050	−0.682					
1560.06	128.99	0.200	0.070	−0.090					
1560.06	97.35	0.190	0.110	0.768					
1672.24	103.47	0.182	0.076	−0.022					
1564.95	107.76	0.156	0.092	0.168					
1503.76	106.28	0.223	0.089	0.211					
1589.83	103.63	0.160	0.130	0.351					
1280.41	159.03	0.240	0.058	0.308					
1587.30	98.26	0.252	0.088	−0.835					

spot size before analysis. In addition, we also discard the first few seconds (and often more – see below) of each analysis to avoid any remaining blank Pb contaminants.

A variety of different calibration strategies for in situ carbonate U–Pb analysis are currently in use. The major problem facing analysts is that, to date, no suitable, homogeneous carbonate reference material has been identified. Most studies, therefore, use the heterogeneous but well-characterized calcite WC-1 (Roberts et al., 2017) and employ a variety of strategies in order to compensate for its heterogeneous nature. For example, Roberts and Walker (2016) use a NIST glass to correct for any bias in $^{207}Pb/^{206}Pb$ ratios and then take a session mean of values for the WC-1 reference material to correct the $^{238}U/^{206}Pb$ ratio of unknowns. They do not perform any downhole fractionation corrections but simply use means of each ablation. Conversely, Hansman et al. (2018) use the NIST glass for correction to both the $^{207}Pb/^{206}Pb$ and $^{238}U/^{206}Pb$ ratios and then apply "additional offset factors" (essentially multipliers) to account for matrix-induced variation in U/Pb ratios between NIST and calcite and downhole fractionation effects.

We have confirmed that there are no observable matrix effects on the $^{207}Pb/^{206}Pb$ ratio when ablating NIST 614 glass relative to calcite and that both return measured / true ratios ≈ 1 within the resolution of our instrument. Therefore, we see no immediate advantage in using a NIST glass in this way and simply use the WC-1 reference material as the primary calibrant. The VizualAge UcomPbine data reduction scheme (DRS; Chew et al., 2014) for Iolite (a popular ICPMS data processing software package; Paton et al., 2011) is designed to allow the use of heterogeneous reference materials (i.e. those with variable amounts of common Pb) such as WC-1 but assumes no $^{207}Pb/^{206}Pb$ fractionation. The time-resolved reference material data from a single spot analysis exhibit shifts in $^{238}U/^{206}Pb$–$^{207}Pb/^{206}Pb$ isochron ("Tera–Wasserburg": Tera and Wasserburg, 1972) space primarily from encountering variable common Pb and/or experiencing downhole Pb/U fractionation. UcomPbine corrects each time slice of background-subtracted data for the reference mate-

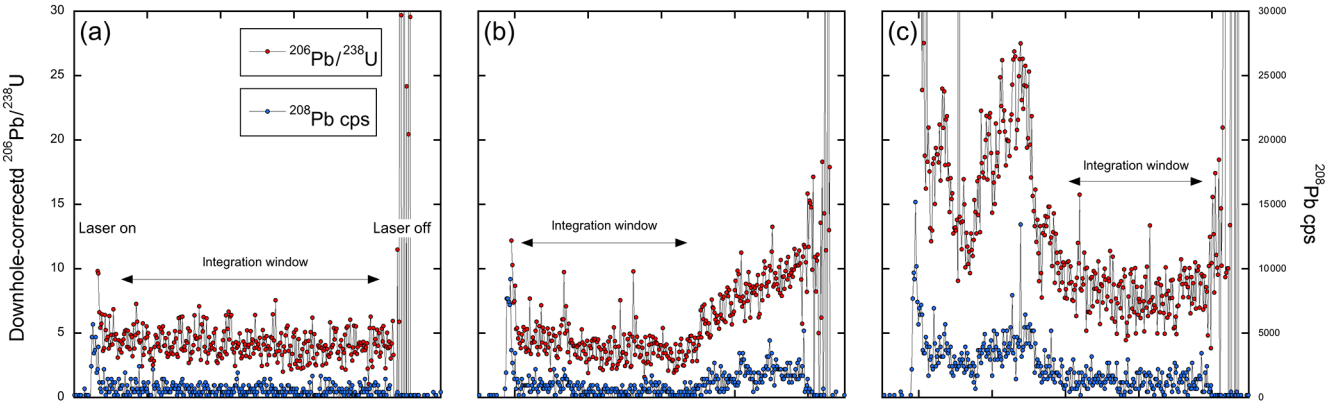

Figure 2. The importance of downhole correction. Panels **(a)**–**(c)** show examples of the complex compositional behaviour seen in many carbonates – these are all single ablations of the same sample. In panel **(a)** a relatively simple structure is observed and, with the exception of a small amount of (surface-contamination) common Pb at the start of the analysis, almost all of the data collected can be used. Panel **(b)** shows a grain with more complex structure and a zone of intrinsic common Pb (high ^{206}Pb/^{238}U and ^{208}Pb cps) encountered towards the end of the ablation, while in **(c)** more common Pb is seen in the first half of the ablation. In complex cases such as these the analyst can focus on the most radiogenic parts of the analysis, as indicated, as long as the data are downhole-corrected.

rial based on its known common and radiogenic Pb compositions using a ^{204}Pb-, ^{207}Pb-, or ^{208}Pb-based approach. This allows the time-resolved radiogenic Pb/U signals to be combined with the ablation depth (or a proxy, such as time since laser on) to correct for downhole Pb/U fractionation as described by Paton et al. (2010). Drift correction is carried out as usual in Iolite by fitting a function (in this case a smoothing spline) to the reference material analyses that bracket unknowns. For this study, the ^{207}Pb-based correction of UcomPbine was employed. Note that the data presented here include only the internal precision for each measurement. The propagated uncertainty of Pb/U ratios can be calculated by UcomPbine using the "pseudo-secondary" approach Iolite uses for its built in U–Pb geochronology DRS (i.e. Paton et al., 2010), but UcomPbine's ^{207}Pb-based correction precludes calculating excess uncertainty on ^{207}Pb/^{206}Pb in this way. We typically find propagated Pb/U uncertainty 1.25 times the internal precision and expect that this factor would be smaller for ^{207}Pb/^{206}Pb. To properly assess the ^{207}Pb/^{206}Pb excess uncertainty and to evaluate mass bias effects which may be more pronounced or resolvable with other instruments, a true secondary reference material with homogeneous ^{207}Pb/^{206}Pb could be employed. As a result of these current limitations, our long-term reproducibility using this methodology is still being evaluated.

We prefer to correct for any downhole elemental fractionation effects, which will be exacerbated with smaller spot sizes. The provision of a downhole correction capacity conveys an important advantage for this type of work in so much as it allows the selection of only the most advantageous areas in a single spot ablation for use, knowing that an appropriate correction for downhole effects has been made at each point in the ablation profile: in other words, the downhole correction allows depth resolution within each individual analysis. This can be a significant benefit in avoiding areas dominated by common Pb which are invariably encountered in the analysis of most carbonates (Fig. 2) and thus maximizing data spread in Tera–Wasserburg space. In addition, this methodology allows us to maximize the use of "good" data, e.g. by trimming only those integrations required at the start of an ablation to remove surface contamination rather than employing a blanket crop of several seconds for every spot analysis. Although the downhole correction profile obtained by Iolite from multiple analyses of a heterogeneous reference material is not as robust as that which might be obtained from a homogeneous reference material, in practice the large numbers of reference analyses included in any given run (at least 16 for the propagation of excess uncertainty) usually produce well-characterized downhole U/Pb profiles when using the UcomPbine DRS.

3 Results and discussion

3.1 The accuracy of the method

In order to assess the accuracy of the method for relatively low-concentration samples we have analysed a number of speleothems for which we have already produced and published ages by solution ID methods (Tables 2 and 3); these display a wide range of radiogenic : common-Pb ratios but, in all cases, have U in the low parts per million range and Pb in the low parts per billion range, typical of many speleothems. In all of these cases the ID data were obtained using a ^{233}U–^{205}Pb isotopic tracer calibrated against EarthTime (http://www.earthtimetestsite.com, last access: 3 December 2019) reference solutions, and accuracy was constantly monitored by reference to EarthTime synthetic zircon solutions run concurrently. The new LA data, together with

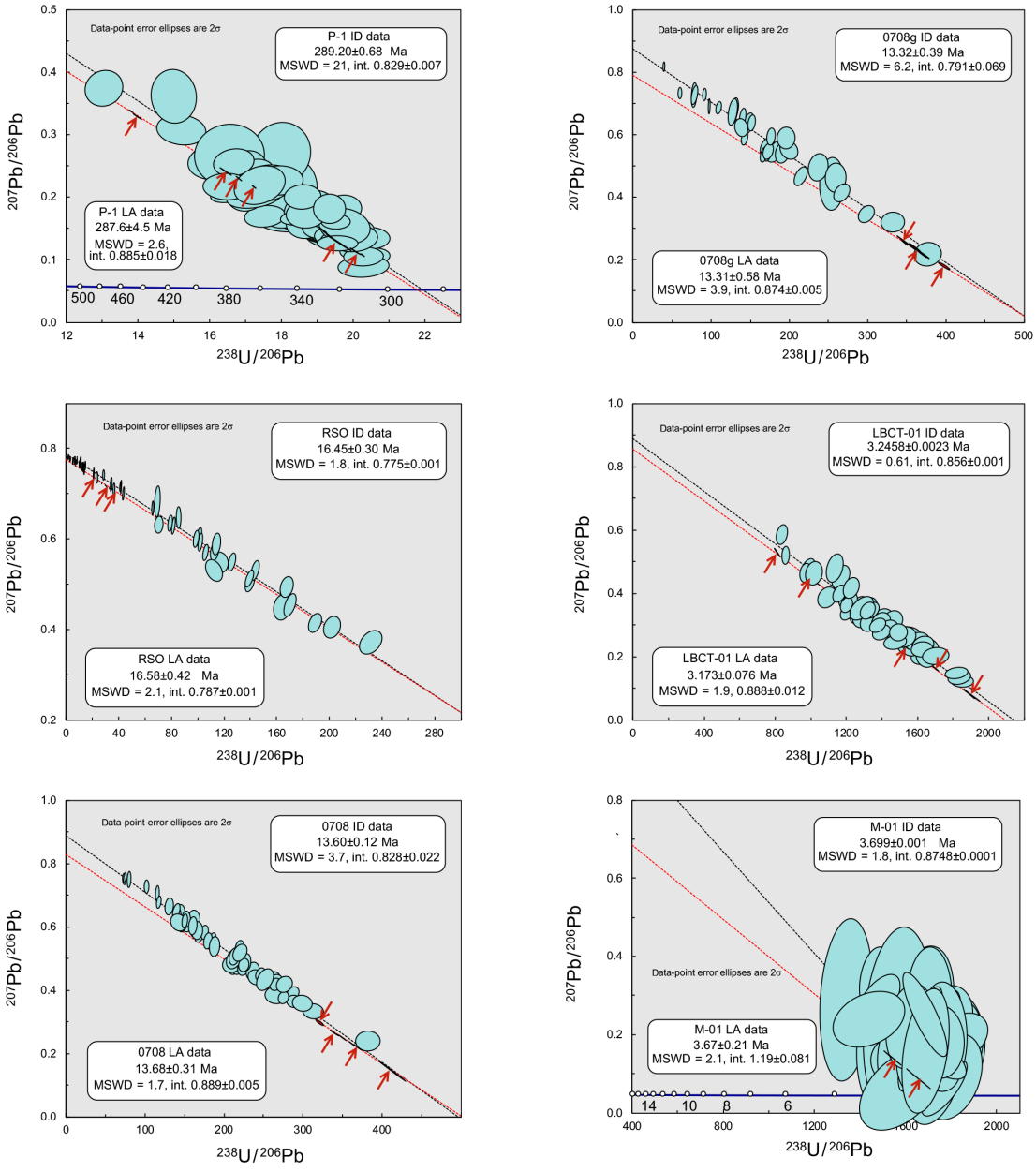

Figure 3. Comparison of ID and LA data. $^{238}U/^{206}Pb$–$^{207}Pb/^{206}Pb$ Tera–Wasserburg isochron plots for key samples analysed in this study. Larger aqua symbols with low error correlations are LA data; smaller red symbols with high levels of error correlation are the isotope dilution data for the same samples – in many cases these are almost invisible at this scale and their locations are, therefore, highlighted with red arrows. Red and black dotted lines represent best-fit isochrons for the LA and ID datasets respectively derived using Isoplot (Ludwig, 2001).

the pre-existing ID data for the same speleothem sample, are presented in the familiar $^{238}U/^{206}Pb$–$^{207}Pb/^{206}Pb$ isochron Tera–Wasserburg construction – see Fig. 3.

It is immediately clear that the LA- and ID-generated data are of quite different character – laser data have inherently large uncertainties resulting from the minute quantities of material being analysed and also show little, if any, error correlation. Mean square of weighted deviate (MSWD) values are in the range of 2–4. In contrast ID data have far smaller individual uncertainties and usually show a high degree of error correlation which is common to many unradiogenic samples plotted in such diagrams. Because of the larger uncertainties shown by the LA data, many more analyses are required in order to constrain an isochron – a feature explored in later discussion.

In all cases shown in Fig. 3 the LA-derived ages fall within uncertainty of the ID-derived data. In addition, for many samples, the LA data show a wider range in U/Pb ratios than the ID data although not consistently more or less radiogenic.

There also appear to be subtle differences in the slope of the isochrons resulting from the two methods: the LA data often (but not always) seem to have a steeper slope and the common-Pb intercepts are not always within uncertainty of each other. We have explored many explanations for this apparent isochron "rotation", including potential inaccuracies in the assumed common-Pb and radiogenic-Pb endmembers for WC-1 and inaccuracies in the calculated dead time used on our instrument (both evaluated by adjustment in post-processing of the data) but find no consistent theme in these studies. As a result of these investigations, and the fact that the effect is variable in occurrence, we currently believe that this effect is most likely attributable to a minute (femtogram) blank contribution from the surface of some samples which is not captured in the baseline (gas blank) measurement and thus cannot be adequately corrected for nor indeed readily measured. Additional tests are underway but, until the exact source of this issue is determined, the $^{207}Pb/^{206}Pb$ intercepts of our LA-derived isochrons must be regarded as inaccurate at the percent level.

It is also clear from these experiments that the LA-generated isochrons rarely attain the high precision of ID datasets – most likely because many orders of magnitude less material is being analysed – although in some cases they certainly approach those values. As such ID-generated data can still be considered the benchmark for high-precision speleothem applications, when abundant suitable sample material is available.

3.2 Number of analyses required and efficiency considerations

Given the relatively large uncertainties associated with each LA analysis, an important consideration in establishing an analytical protocol is the number of analyses required to form a robust age determination. In order to assess the effect of sample size on isochron quality, we collected large numbers of spot analyses (up to 70) for several samples and then randomly subsampled this dataset, determining the age at each step. All samples show very similar behaviour, and so we use, as an example, results for sample P-1 in Fig. 4.

A somewhat unexpected observation from this analysis is that relatively high-accuracy and high-precision ages can be obtained with as few as 30 spot analyses and that any subsequently acquired data often do little to improve the analytical precision. There is, however, considerable scope for generating erroneous ages with analysis counts lower than ~ 30.

These data feed into an assessment of the potential time savings available from LA analysis compared to ID studies. If we assume 30 spot analyses "per age" this amounts

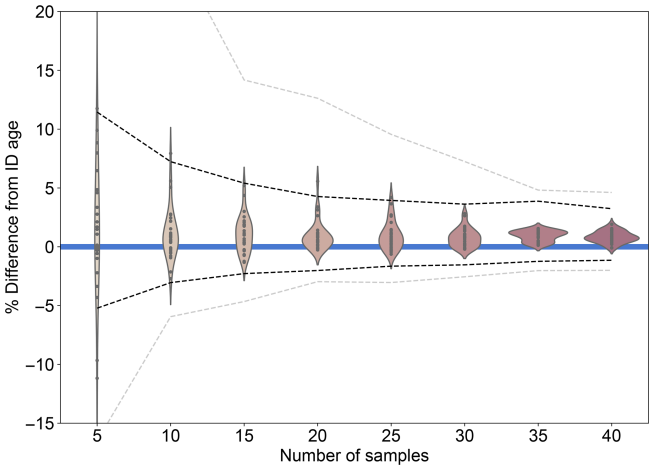

Figure 4. Sample size vs. isochron quality. Percent difference of LA intercept age from ID age versus sample size when randomly subsampling the P-1 dataset. Thirty different random selections of these data were made for each sample size. The resulting intercept ages for each of the selections are represented individually as dots and collectively as a vertical kernel density estimate ("violin plot"). The ID age with uncertainty is represented by the blue bar centred on ordinate 0. The black and grey dashed lines are the median and extreme uncertainties calculated for each sample size.

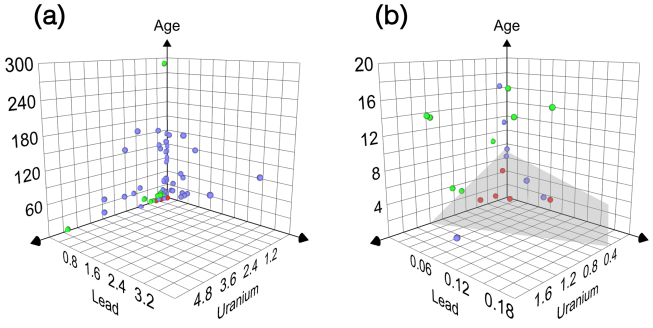

Figure 5. Limitations of the method. Plots of U and Pb contents vs. age for our own samples and those literature studies from which concentration data could be extracted, with panel **(b)** representing a zoom view of the data shown in panel **(a)**. Data points represent the average of concentrations reported for each sample: for our own analyses these are ID analyses but, in the case of literature samples, these are the concentration data reported from LA studies. Samples are colour-coded – those in purple represent successful literature age determinations by LA methodologies, whereas those in green are our own successful LA analyses. Samples shown in red, however, are those for which we have previously successfully determined ID ages but have not been able to produce isochrons using LA. These samples we consider to be beyond the current limits of the LA technique due to a combination of low U and Pb contents and age. A grey plane is drawn to separate successful from unsuccessful analyses. Data sources: this study, Li et al. (2014), Coogan et al. (2016), Ring and Gerdes (2016), Roberts and Walker (2016), and Hansman et al. (2018).

to around 40 min run time per sample using our analytical protocol.

Once sample preparation time (slabbing and polishing or resin mounting) and other overheads (e.g. digitizing, cell stabilization after sample changes) are taken into account, however, it may be hard to generate more than 10–20 age determinations per week without significant automation such as overnight running. In comparison, we tend to process aliquots for ID studies in batches of 30 which routinely provides approximately five age determinations per week (1 d sample preparation and cleaning, 1 d spiking, 1 d chemistry, and 2 d mass spectrometry), with clear scope for further expansion. There is certainly, therefore, significant time saving when employing LA analysis but not necessarily a dramatic (order of magnitude) one. As such LA methods offer great potential as a rapid reconnaissance tool, largely superseding alternative methods advocated by Woodhead et al. (2012).

3.3 Limitations of the method

In addition to the small number of isochrons shown here for samples with published ID-derived ages, we have throughout the course of this study attempted to reproduce our ID-derived ages for a number of other (currently unpublished) samples of variable age and U and Pb contents. The results of these experiments, combined with comparable data gathered from literature studies of non-spelean carbonates, are plotted in Fig. 5. In this plot, samples are colour-coded – those in purple represent successful literature age determinations by LA methodologies, whereas those in green are our own successful LA analyses. The diagram illustrates the particular challenges of analysing speleothem materials compared with many other carbonates – sub-parts per million levels of U and Pb and generally relatively young ages. Samples shown in red are those for which we have previously successfully determined ID ages but have not been able to produce isochrons using LA. These samples we consider to be beyond the current limits of the LA technique due to a combination of low U and Pb contents and age.

We recognize that the results of such an entirely empirical approach are likely to show some variation between instrumentation and may ultimately change as equipment becomes more sensitive; for the moment, however, this diagram provides a first impression as to the potential limitations of the method as judged by current literature data. A relatively simple plane can be drawn to separate "successful" from "unsuccessful" experiments: the equation of this plane in x (U ppm) $-y$ (Pb ppm) $-z$ (age in Ma) space is $2.25x + 10.5y + 0.42z - 3.15 = 0$. If the analyst has an independent assessment of likely U and Pb contents (e.g. from reconnaissance quadrupole ICPMS analyses) and an approximate idea of age, these values can be inserted into the equation above. Strongly positive values would suggest a high likelihood of dating success with appropriate equipment, whereas negative values would suggest parameters likely to

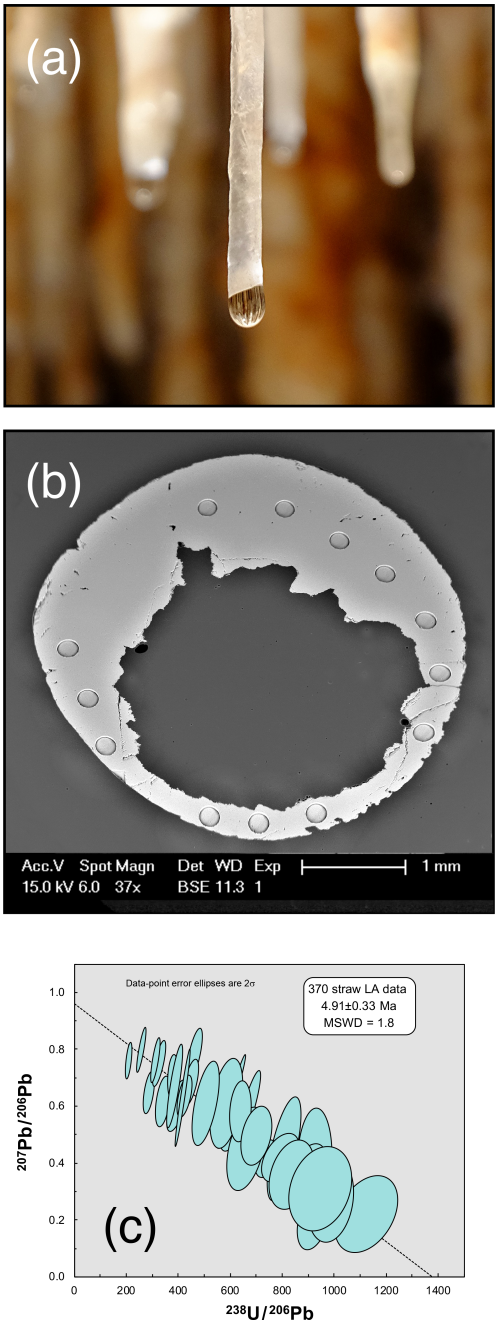

Figure 6. An example of high spatial-resolution geochronology. High spatial-resolution analysis of a straw speleothem from the Nullarbor Plain of SW Australia. Panel **(a)** shows an active straw stalactite in situ, while panel **(b)** is an SEM cross-sectional view of the sample studied showing typical dimensions and wall thickness, together with representative laser ablation pits. Panel **(c)** shows the Tera–Wasserburg isochron which is within the range of other speleothems analysed from this site via ID methods (Woodhead et al., 2019).

be beyond the current reach of the methodology. In broader terms any samples with > 1 ppm U and a few hundred parts per billion of Pb should be datable regardless of age. The actual range of U/Pb ratios present in a sample also plays a role in the generation of isochrons, but almost all carbonate materials analysed to date show some variation in this ratio at the micron scale, and thus the potential for isochron construction if isotopic measurement of their U and Pb is analytically feasible.

3.4 Advantages of the method

It is clear from the previous discussion that the LA methodology has some limitations in terms of working with small amounts of U or Pb or relatively young samples. In comparison, ID methods can produce useful data from samples with lower U and Pb concentrations simply because of the much larger sample sizes employed (typically 50 mg for a bulk ID analysis compared with 0.005 mg for an LA analysis). As a result, higher-precision data can be obtained and consequently, younger samples can be dated – samples in the range of a few hundred thousand years are possible by ID (e.g. Richards et al., 1998), providing substantial overlap with the U–Th chronometer in optimal circumstances.

The trade-off, however, is one of spatial resolution – LA methods offer a few hundred microns resolution compared to several millimetres (at best) using samples drilled out for ID analysis. Note in this context that it is difficult to produce sample powders for U–Pb analysis without contamination by environmental Pb, and so traditional micro-milling methodologies are not applicable to low-level Pb samples. For this reason, in speleothem studies, complete fragments of crystalline calcite have to be removed by drilling (Woodhead et al., 2006, 2012). The power of these high spatial-resolution LA approaches has already been demonstrated by previous studies, e.g. an analysis of single calcite fibres in vein structures (e.g. Goodfellow et al., 2017). Here we use an example from speleothem studies.

Straw stalactites – hollow, calcite cylinders that precipitate from cave drip points – are thin-walled structures which are plentiful in many caves and often form the nucleation point for the eventual growth of stalactites. Because of their fast-growing habit, they have been explored as short-term climate records (e.g. Paul et al., 2013) but they are also rather fragile and frequently broken off. Because of this they readily accumulate in cave sediments and have been shown to be useful in the context of dating relatively young archaeological sequences at cave sites via the U–Th method (St Pierre et al., 2009). Cave straws are in fact often remarkably well preserved and so could be used to date many cave sedimentary sequences of any age, but no previous attempts have been made to obtain U–Pb ages for these due to their minute size.

In Fig. 6 we show a straw speleothem from the roof of a Nullarbor cave which has been shown to contain speleothems in the 3.1–5.6 Ma range (Woodhead et al., 2019). This sample has a total diameter of only ∼ 5 mm and a wall thickness of between 0.25 and 1.2 mm (Fig. 5b). In addition, the outer regions of straws (those areas exposed to the environment) can contain high levels of detrital components derived from dust. Dating of such structures would be impossible by conventional ID methods, but we are able to use the laser to obtain a well-constrained isochron age of 4.91 ± 0.33 Ma (uncorrected for initial disequilibrium). It is impossible in this case to independently confirm the validity of this age, but it is well within the range of nearby cave formations previously dated by ID.

In addition to the ability to date extremely small and/or fragile materials, the increased spatial resolution afforded by the laser provides a further advantage – a greatly increased ability to avoid areas dominated by common-Pb and/or open-system behaviour which may be unavoidable in ID analyses where ∼ 50 mg calcite samples are the norm. As a result, there are likely to be many situations where laser approaches can produce age information for samples which are intractable to ID approaches.

4 Conclusions

Laser ablation methods are capable of generating accurate U–Pb ages for speleothems (and by inference other carbonates) with moderate U contents (> 1 ppm), regardless of age. At lower U contents, however, the possibility of successful outcomes is also strongly dependent on Pb content and age. Together with our own studies, a compilation of successful literature analyses provides a first-order test for potential dating suitability. The absolute precision obtained by LA methods can approach but rarely supersedes that of the benchmark ID method. The latter, however, requires many orders of magnitude more sample to achieve. LA conveys an advantage in speed and is thus useful as a reconnaissance tool. The overwhelming advantage of LA methods, however, remains one of high spatial resolution, allowing the dating of materials which are beyond the reach of ID methods simply because of their size.

Data availability. The raw Attom data and RESOlution laser log files for the LA analyses and the Iolite-3 experiments showing how they were processed can be obtained from the authors.

Author contributions. JW collected the analytical data. JW and JP both performed the data analysis and wrote the paper.

Competing interests. The authors declare that they have no conflict of interest.

Special issue statement. This article is part of the special issue "In situ carbonate U–Pb geochronology". It is a result of the Goldschmidt conference, Barcelona, Spain, 18–23 August 2019.

Acknowledgements. We thank Matt Horstwood and Chris Smith for convincing us that in situ dating of speleothems was actually feasible long before we had an appropriate mass spectrometer to experiment ourselves. Nick Roberts provided the WC-1 reference material and, together with Phil Shaw and Ariane Donard of Nu Instruments, advised on instrumental matters. Graham Hutchinson produced the SEM images.

Financial support. This research has been supported by the Australian Research Council (grant no. FL160100028).

Review statement. This paper was edited by Perach Nuriel and reviewed by Matthew Horstwood and one anonymous referee.

References

Chew, D. M., Petrus, J. A., and Kamber, B. S.: U–Pb LA–ICPMS dating using accessory mineral standards with variable common Pb, Chem. Geol., 363, 185–199, 2014.

Coogan, L. A., Parrish, R. R., and Roberts, N. M. W.: Early hydrothermal carbon uptake by the upper oceanic crust: insight from in situ U-Pb dating, Geology, 44, 147–150, 2016.

Drost, K., Chew, D., Petrus, J. A., Scholze, F., Woodhead, J. D., Schneider, J. W., and Harper, D. A. T.: An Image Mapping Approach to U-Pb LA-ICP-MS Carbonate Dating and Applications to Direct Dating of Carbonate Sedimentation. Geochem. Geophy. Geosy., 19, 4631–4648, 2018.

Goodfellow, B. W., Viola, G., Bingen, B., Nuriel, P., and Kylander-Clark, A. R. C.: Palaeocene faulting in SE Sweden from U-Pb dating of slickenfibre calcite, Terra Nova, 29, 321–328, 2017.

Hansman, R. J., Albert, R., Gerdes, A., and Ring, U.: Absolute ages of multiple generations of brittle structures by U-Pb dating of calcite, Geology, 46, 207–210, 2018.

Jahn, B.-M. and Cuvellier, H.: Pb-Pb and U-Pb geochronology of carbonate rocks: an assessment, Chem. Geol., 115, 125–151, 1994.

Li, Q., Parrish, R. R., Horstwood, M. S. A., and McArthur, J. M.: U-Pb dating of cements in Mesozoic ammonites, Chem. Geol., 376, 76–83, 2014.

Ludwig, K. R.: Isoplot/Ex, rev. 2.49. A Geochronological Toolkit for Microsoft Excel, Berkeley Geochronology Center Special Publication 1a, 2001.

Lundberg, J., Ford, D. C., and Hill, C. A.: A preliminary U-Pb date on cave spar, Big Canyon, Guadalupe Mountains, New Mexico, U.S.A., J. Cave Karst Stud., 62, 144–148, 2000.

Meyer, M. C., Cliff, R. A., and Spötl, C.: Speleothems and mountain uplift, Geology, 39, 447–450, 2011.

Moorbath, S., Taylor, P. N., Orpen, J. L., Treloar, P., and Wilson, J. F.: First direct dating of Archaean stromatolitic limestone, Nature, 326, 865–867, 1987.

Parrish, R. R., Parrish, C. M., and Lasalle, S.: Vein calcite dating reveals Pyrenian orogen as cause of Paleogene deformation in southern England, J. Geol. Soc. London, 175, 425–442, 2018.

Paton, C., Woodhead, J. D., Hellstrom, J. C., Hergt, J. M., Greig, A., and Maas, R.: Improved laser ablation U-Pb zircon geochronology through robust downhole fractionation correction, Geochem. Geophy. Geosy., 11, https://doi.org/10.1029/2009GC002618, online first, 2010.

Paton, C., Hellstrom, J., Paul, B., Woodhead, J., and Hergt, J.: Iolite: Freeware for the visualisation and processing of mass spectrometric data, J. Anal. Atom. Spectrom., 26, 2508–2518, 2011.

Paul, B., Drysdale, R., Green, H., Woodhead, J., Hellstrom, J., and Eberhard, R.: A model for the formation of layered soda-straw stalactites, Int. J. Speleol., 42, 155–160, 2013.

Pickering, R., Dirks, P. H. G. M., Jinnah, Z., de Ruiter, D. J., Churchill, S. E., Herrires, A. I. R., Woodhead, J. D., Hellstrom, J. C., and Berger, L. R.: *Australopithecus sediba* at 1.977 Ma and implications for the origins of Genus Homo, Science, 333, 1421–1423, 2011.

Pickering, R., Herries, A. I. R., Woodhead, J. D., Hellstrom, J. C., Green, H. E., Paul, B., Ritzman, T., Strait, D. S., Schoville, B. J., and Hancox, P. J.: U-Pb dated flowstones restrict South African early hominin record to dry climate phases, Nature, 565, 226–229, 2019.

Polyak, V., Hill, C., and Asmeron, Y.: Age and evolution of the Grand Canyon revealed by U-Pb dating of water-table-type speleothems, Science, 319, 1377–1380, 2008.

Rasbury, E. T. and Cole, J. M.: Directly dating geologic events: U-Pb dating of carbonates, Rev. Geophys., 47, RG3001, https://doi.org/10.1029/2007RG000246, 2009.

Richards, D. A., Bottrell, S. H., Cliff, R. A., Strohle, K., and Rowe, P. J.: U-Pb dating of a speleothem of Quaternary age, Geochim. Cosmochim. Ac., 62, 3683–3688, 1998.

Ring, U. and Gerdes, A.: Kinematics of the Alpenrhein-Bodensee graben system in the Central Alps: Oligocene/Miocene transtension due to formation of the Western Alps arc, Tectonics, 35, 1367–1391, https://doi.org/10.1002/2015TC004085, 2016.

Roberts, N. M. W. and Walker, R. J.: U-Pb geochronology of calcite-mineralized faults: absolute timing of rift-related fault events on the northeast Atlantic margin, Geology, 44, 531–534, 2016.

Roberts, N. M. W., Rasbury, E. T., Rarrish, R. R., Smith, C. J., Horstwood, M. S. A., and Condon, D. J.: A calcite reference material for LA-ICP-MS U-Pb geochronology, Geochem. Geophy. Geosy., 18, 2807–2814, doi.org/10.1002/2016GC006784, 2017.

Sniderman, J. M. K., Woodhead, J. D., Hellstrom, J., Jordan, G. J., Drysdale, R. N., Tyler, J. J., and Porch, N.: Pliocene reversal of late Neogene aridification, P. Natl. Acad. Sci, USA, 113, 1999–2004, 2016.

St Pierre, E., Zhao, J.-X., and Reed, E.: Expanding the utility of Uranium-series dating of speleothems for archaeological and palaeontological applications, J. Archaeol. Sci., 36, 1416–1423, 2009.

Tera, F. and Wasserburg, G. J.: U- Th- Pb systematics in three apollo 14 basalts and the problem of initial Pb in Lunar rocks, Earth Planet. Sc. Lett., 14, 281–304, 1972.

Vaks, A., Woodhead, J. D., Bar-Matthews, M., Ayalon, A., Cliff, R. A., Zilberman, T., Matthews, A., and Frumkin, A.: Pliocene-Pleistocene climate of the northern margin of Saharan-Arabian

Desert recorded in speleothems from the Negev Desert, Israel, Earth Planet. Sc. Lett., 368, 88–100, 2013.

Walker, J., Cliff, R. A., and Latham, A. G.: U-Pb isotopic age of the StW 573 2059 hominid from Sterkfontein, South Africa, Science, 314, 1592–1594, 2006.

Woodhead, J., Reisz, R., Fox, D., Drysdale, R., Hellstrom, J., Maas, R., Cheng, H., and Edwards, R. L.: Speleothem climate records from deep time? Exploring the potential with an example from the Permian, Geology, 38, 455–458, 2010.

Woodhead, J., Hellstrom, J., Pickering, R., Drysdale, R., Paul, B., and Bajo, P.: U and Pb variability in older speleothems and strategies for their chronology, Quat. Geochronol., 14, 105–113, 2012.

Woodhead, J., Hand, S., Archer, M., Graham, I., Sniderman, K., Arena, D. A., Black, K., Godthelp, H., Creaser, P., and Price, E.: Developing a radiometrically-dated chronologic sequence for Neogene biotic change in Australia, from the Riversleigh World Heritage Area of Queensland, Gondwana Res., 29, 153–167, 2016.

Woodhead, J. D., Hellstrom, J., Maas, R., Drysdale, R., Zanchetta, G., Devine, P., and Taylor, E.: U-Pb geochronology of speloethems by MC-ICPMS, Quat. Geochronol., 1, 208–221, 2006.

Woodhead, J. D., Sniderman, J. M. K., Hellstrom, J., Drysdale, R. N., Maas, R., White, N., White, S., and Devine, P.: The antiquity of Nullarbor speleothems and implications for karst palaeoclimate archives, Sci. Rep., 9, 603, https://doi.org/10.1038/s41598-018-37097-2, 2019.